Geochemistry Geophysics Geosystems G3
Article
Volume 14, Number 6
6 June 2013
doi:10.1002/ggge.20121
ISSN: 1525-2027
Published by AGU and the Geochemical Society

Rapid eruption of the Ningwu volcanics in eastern China: Response to Cretaceous subduction of the Pacific plate

Yan-Jie Tang
State Key Laboratory of Lithospheric Evolution, Institute of Geology and Geophysics, Chinese Academy of Sciences, P.O. Box 9825, No. 19, Beitucheng Western Road, Chaoyang District, Beijing 100029, China (tangyanjie@mail.igcas.ac.cn)

Hong-Fu Zhang
State Key Laboratory of Lithospheric Evolution, Institute of Geology and Geophysics, Chinese Academy of Sciences, P.O. Box 9825, No. 19, Beitucheng Western Road, Chaoyang District, Beijing 100029, China

State Key Laboratory of Continental Dynamics, Department of Geology, Northwest University, No. 229, Taibai Northern Road, Beilin District, Xi'an 710069, China

Ji-Feng Ying, Ben-Xun Su, and Xian-Hua Li
State Key Laboratory of Lithospheric Evolution, Institute of Geology and Geophysics, Chinese Academy of Sciences, P.O. Box 9825, No. 19, Beitucheng Western Road, Chaoyang District, Beijing 100029, China

M. Santosh
School of Earth Science and Resources, China University of Geosciences, No. 29, Xueyuan Road, Haidian District, Beijing 100083, China

[1] The relationship between lithospheric evolution of eastern Eurasia and subduction of the Pacific plate has long been debated. However, the timing and implications of subduction on the tectonics of eastern China are not well constrained. Here we present new zircon U-Pb ages and Hf isotopes, elemental and Sr-Nd-Pb isotopic data on Cretaceous volcanic rocks from the Ningwu basin, eastern China to further address this issue. Our age data reveal rapid eruption of the volcanic rocks within a short duration from 133 to 130 Ma. The rocks, mostly characterized by shoshonitic and high-K calc-alkaline signatures, display light rare earth element and Pb enrichment, Nb, Ta and Ti depletion, highly radiogenic Sr-Pb isotopic ratios and variable $\varepsilon_{Hf}(t)$ (+1.8 to -10), suggesting derivation from an enriched lithospheric mantle metasomatized by marine sediments. The early lavas (133.3 ± 1.1 Ma) show stronger subduction-related signatures than the late lavas (130.1 ± 1.0 Ma), which we interpret to reflect consumption of a significant volume of fusible subducted components in the early melting phase. The large $\varepsilon_{Hf}(t)$ variation of late lavas suggests greater involvement of asthenospheric melts and lower crust in their petrogenesis. The youngest age (130 Ma) appears to coincide with an inferred change in the direction of Pacific-Eurasia convergence, manifested as a change from extension to transpression in eastern China. The narrow window of eruption may signify a rapid change of the tectonic regime in the Early Cretaceous.

Components: 10,200 words, 10 figures, 3 tables.

Keywords: U-Pb age; geochemistry; lithospheric evolution; Eastern China; pacific plate subduction.

Index Terms: 1031 Geochemistry: Subduction zone processes (3060, 3613, 8170, 8413); 1038 Geochemistry: Mantle processes (3621); 1065 Geochemistry: Major and trace element geochemistry; 1040 Geochemistry: Radiogenic isotope geochemistry; 1115 Geochronology: Radioisotope geochronology.

Received 8 January 2013; **Revised** 4 March 2013; **Accepted** 17 March 2013; **Published** 6 June 2013.

Tang, Y.-J., H.-F. Zhang, J.-F. Ying, B.-X. Su, X.-H. Li, and M. Santosh (2013), Rapid eruption of the Ningwu volcanics in eastern China: Response to Cretaceous subduction of the Pacific plate, *Geochem. Geophys. Geosyst.*, *14*, 1703–1721, doi:10.1002/ggge.20121.

1. Introduction

[2] Eastern China is well known for the transformation of an ancient, thick (~ 200 km), cold, and refractory lithospheric mantle into a relatively young, thin (<80 km), hot, and fertile one since the Paleozoic [cf. *Xu*, 2001]. The lithospheric thinning, accompanied by the Cretaceous giant igneous event [*Wu et al.*, 2005] and large-scale lode gold mineralization [*Mao et al.*, 2011] in eastern China has been interpreted to have been caused by lithospheric extension [*Li*, 2000], subduction-related transpression [*Zhou and Li*, 2000], thermo-mechanical and chemical erosion [*Xu*, 2001], peridotite-melt interaction [*Zhang*, 2005], lithospheric replacement [*Gao et al.*, 2002; *Zheng et al.*, 2006], crustal delamination [*Gao et al.*, 2004], and other processes [*Zhang et al.*, 2013 and references therein]. The large-scale mineralization in eastern China is considered to have formed during lithospheric thinning, likely controlled by the subduction of the Pacific plate [*Sun et al.*, 2007; *Mao et al.*, 2011].

[3] Eastern Eurasia became an active continental margin from the Jurassic to the Cretaceous, closely associated with subduction of the Pacific plate [*Li and Li*, 2007; *Sun et al.*, 2007]. Multiple lines of evidence suggest that subduction of the Pacific plate strongly influenced geological processes in eastern China [*Zhou and Li*, 2000; *Wu et al.*, 2005; *Sun et al.*, 2007; *Liu et al.*, 2010; *Santosh et al.*, 2010; *Mao et al.*, 2011; *Tang et al.*, 2012; *Zhu et al.*, 2012]. However, the timing of subduction and contribution of Pacific plate to lithospheric evolution in eastern China are not fully constrained due to the lack of systematic and high precision age data and comprehensive studies on geochronology and geochemistry. In this study, we present precise SIMS U-Pb zircon age, Hf isotope data, major and trace elements, and Sr, Nd, and Pb isotopes on a suite of Cretaceous volcanic rocks from the Ningwu basin, eastern China. Our results provide new insights into the petrogenesis of the Cretaceous volcanism in eastern China and the intrinsic relationship between the lithospheric evolution and subduction of the Pacific plate.

2. Geologic Setting

[4] The Ningwu (Nanjing-Wuhu; Figure 1) basin is situated at the northeastern margin of the Yangtze Craton, which is separated from the North China Craton by the Dabie-Sulu orogenic belt. This orogen hosts the largest known ultra–high-pressure metamorphic belt on Earth [*Yang*, 2002], and was formed by northward subduction of the Yangtze Craton beneath the North China Craton in the Triassic [*Li et al.*, 1993; *Wu and Zheng*, 2013]. The Ningwu basin is a NNE-trending Late Mesozoic volcanic basin in the Lower Yangtze River region, eastern China. As a part of the western circum-Pacific metallogenic belt, the Lower Yangtze River region is one of the most important Late Mesozoic magmatic and metallogenic belts in the eastern Eurasian continental margin [*Mao et al.*, 2011]. The Ningwu basin has received considerable attention owing to the discovery of abundant iron deposits, including the world-class Meishan, Washan and Gushan deposits, leading to several investigations on the ore deposits and magmatic suite in the Ningwu basin [*Mao et al.*, 2011, and references therein].

[5] Volcanic rocks in the Ningwu basin cover ~1000 km^2 and are mainly composed of trachy-andesite, andesite, trachyte, dacite, breccia, and tuff, with minor alkaline basalt, basaltic andesite, rhyolite and phonolite. They are divided into four formations: Longwangshan, Dawangshan, Gushan and Niangniangshan from the base to top (Figure 1; the Gushan Formation is not shown in the stratigraphic section due to seldom exposure). The Longwangshan Formation volcanic rocks cover ~200 km^2 and unconformably overlie Triassic and Jurassic sedimentary rocks. The Longwangshan Formation is mainly composed of lavas and pyroclastic rocks, with compositions of hornblende-bearing andesite and trachy-andesite, and is distributed along the eastern margin of the basin. The Dawangshan Formation volcanic rocks are mainly composed of trachyte, trachy-andesite, andesitic volcanic rock, tuff, and lava. They are widespread in the basin, covering ~750 km^2. In contrast, the exposures of Gushan and Niangniangshan Formations are very limited (< 50 km^2). The Gushan Formation is mainly exposed in the southern part of the basin and composed of andesite and andesitic pyroclastic rocks. The Niangniangshan Formation is exposed in the western margin of the basin and mainly consists of conglomerate, breccia, and phonolitic breccia tuff.

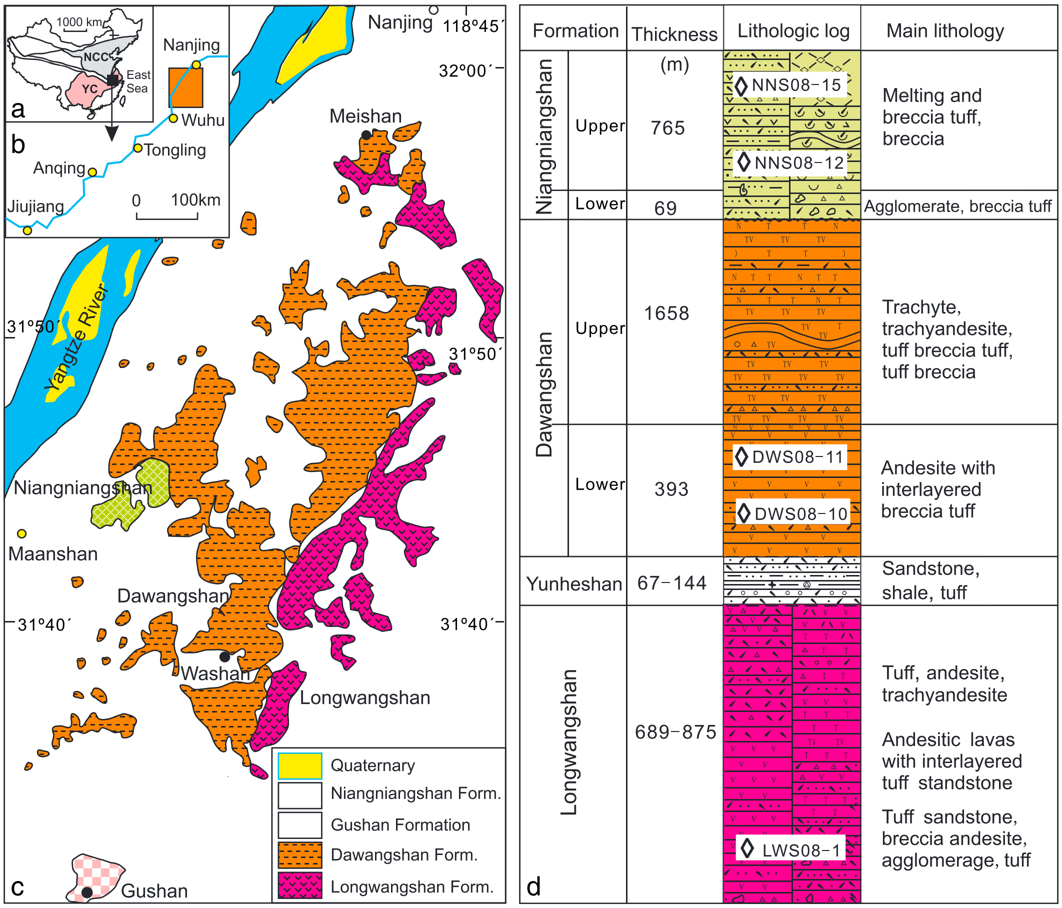

Figure 1. (a) Location of the North China Craton (NCC) and Yangtze Craton (YC), (b) location of the Ningwu basin, (c) distribution of Cretaceous volcanic rocks in the Ningwu basin, and (d) stratigraphic section of the Ningwu basin, Lower Yangtze River region, eastern China, showing sample locations.

3. Previous Studies and Sample Description

[6] The Ningwu volcanic rocks are intermediate-mafic, mostly shoshonites, with high-K and calc-alkaline series. The Nd and Sr isotopic data compiled from previous studies on the Mesozoic Na-enriched (alkaline mafic) and K-enriched rocks in the Lower Yangtze River region indicate that the mantle beneath this region is characterized by enriched isotopic signatures [*Chen et al.*, 2001]. The geochemical data for the Cretaceous basalt, gabbro, and diorite from this region suggest that the mantle sources were metasomatized by ancient slab-derived material and the rocks possibly formed by the mixing of melts from isotopically enriched lithospheric mantle and depleted asthenosphere [*Yan et al.*, 2008]. However, some studies suggested that the parental magmas for the Ningwu volcanic rocks were mainly derived from an enriched lithospheric mantle and underwent contamination by continental crust rocks, during a phase of lithospheric extension [*Wang et al.*, 2001; *Hou and Yuan*, 2010].

[7] Early published age data of K-Ar dating and Rb-Sr isochron for the Ningwu volcanic rocks show a wide variation from 136 to 91 Ma [*Yan et al.*, 2009, and references therein]. The reported SHRIMP zircon U-Pb ages for the Longwangshan and Dawangshan Formations are 131 ± 4 Ma and 127 ± 3 Ma [*Zhang et al.*, 2003a]. LA-ICPMS zircon U-Pb dating shows variable ages for the Niangniangshan Formation, from 133 ± 3 to 128 ± 3 Ma, with weighted mean ages of 130.6 ± 1.1 Ma [*Yan et al.*, 2009], 130.3 ± 0.9 Ma for the Dawangshan Formation, and 128.5 ± 1.8 Ma for the Gushan Formation [*Hou and Yuan*, 2010]. Recently reported LA-ICPMS zircon U-Pb ages for the Longwangshan, Dawangshan, Gushan, and Niangniangshan Formations are 134.8 ± 1.3, 132.2 ± 1.6, 129.5 ± 0.8, and 126.6 ± 1.1 Ma, respectively [*Zhou et al.*, 2011]. These results are almost consistent within analytical errors and show

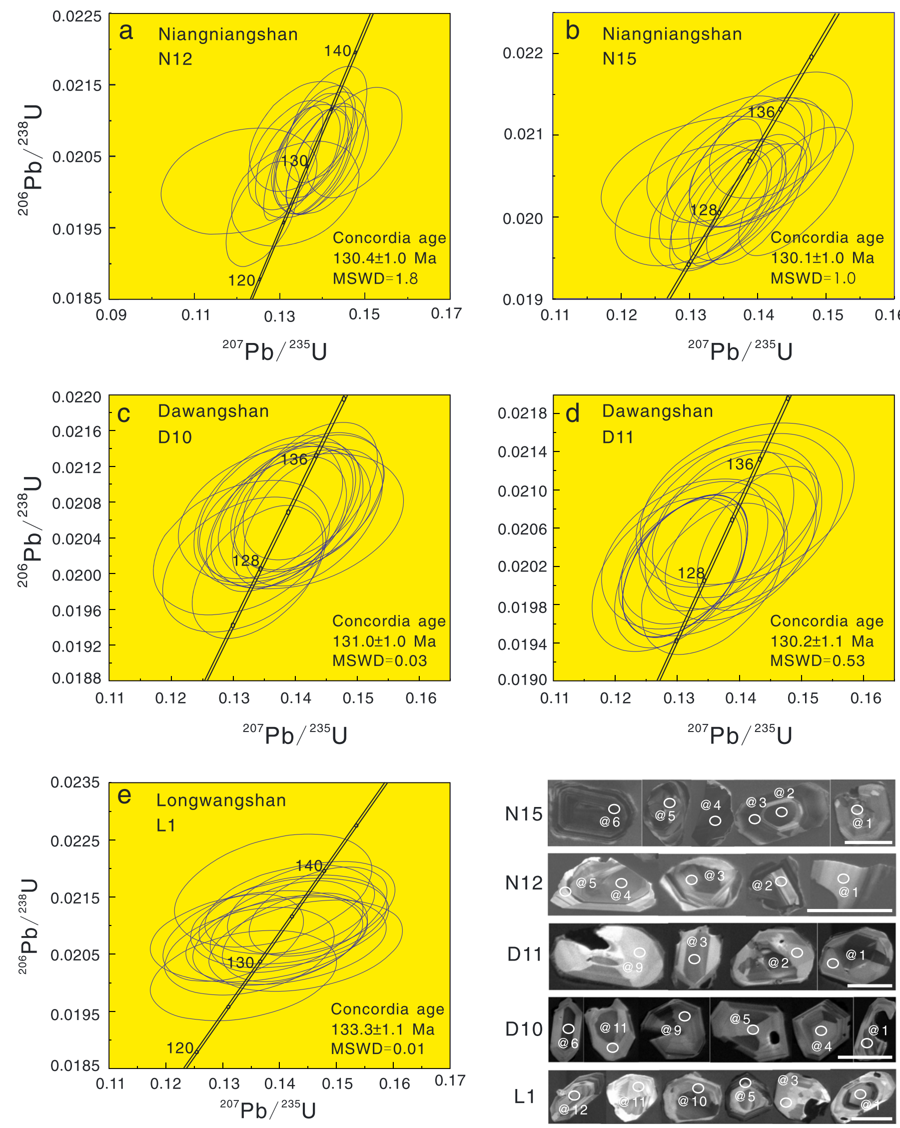

Figure 2. SIMS U-Pb concordia age plots and cathodoluminescence (CL) images of zircons from the Ningwu lavas. The white ellipses in the CL images represent the spots of SIMS analyses. The white bars are 100 μm in length for scale. Data-point error ellipses are 2σ.

that all the volcanic rocks formed in the Early Cretaceous. However, high precision age data for the volcanic rocks are few.

[8] Fresh volcanic rocks were sampled from the Longwangshan, Dawangshan, and Niangniangshan Formations. These samples are mainly composed of trachy-andesite, trachyte, and trachy-dacite. The trachy-andesites show porphyritic texture with phenocrysts predominantly of plagioclase, minor augite, and hornblende. The plagioclase and augite phenocrysts show reaction or resorption rims, which commonly result from magma mixing between mafic and felsic melts [*Anderson*, 1976]. The matrix has a very fined-grained texture and is composed predominantly of plagioclase with subordinate K-feldspar. The trachytes are massive, and display porphyritic texture with phenocrysts of plagioclase, K-feldspar, amphibole and minor hornblende. The matrix consists mainly of glass with sparse crystallites of plagioclase, amphibole and magnetite. One rhyolite sample (D11) has phenocrysts of quartz, K-feldspar, and minor oligoclase and biotite, and the matrix is mainly glass with feldspar, quartz, and biotite.

4. Analytical Methods

[9] Zircons were separated by conventional magnetic and density techniques and then handpicked and mounted in transparent epoxy resin together with

Table 1. Chemical Compositions of Volcanic Rocks From the Ningwu Basin

	Longwangshan						Dawangshan					Niangniangshan									
Formation Sample No.	L1	L2	L3	L4	L5	L7	D10	D11	D22	D23	D25	N12	N13	N14	N15	N16	N17	N18	N19	N20	N21
Major elements (wt %)																					
SiO_2	56.94	59.97	61.54	57.92	50.43	56.28	66.21	70.22	60.68	61.17	60.98	60.94	61.78	61.08	60.45	63.58	62.22	60.51	62.96	60.29	61.58
Al_2O_3	15.77	18.16	15.21	18.40	20.84	17.94	17.64	15.50	18.40	18.66	18.50	18.83	19.77	19.05	18.28	13.54	13.48	14.97	13.41	18.58	19.29
Fe_2O_3	13.42	9.87	9.78	7.27	9.26	8.55	8.74	2.54	3.07	2.79	2.79	2.96	2.82	3.09	3.04	7.55	5.85	8.13	9.20	3.14	2.46
MgO	0.11	0.13	0.27	1.21	1.78	1.85	0.12	0.27	0.84	0.47	0.47	0.59	0.42	0.81	1.03	1.00	1.25	1.11	0.60	0.31	0.39
CaO	0.29	0.37	0.32	0.76	2.11	1.52	1.37	0.32	2.21	1.96	2.06	1.71	0.54	1.50	2.13	1.33	2.45	2.82	0.56	1.95	1.11
Na_2O	0.28	0.26	0.26	3.86	4.21	2.88	0.07	4.08	5.47	5.87	6.05	5.15	3.66	4.58	5.39	5.39	4.40	5.89	3.85	5.05	4.94
K_2O	9.61	7.03	8.84	6.03	6.36	7.35	3.60	4.70	6.81	6.94	7.04	7.22	7.56	6.89	6.54	3.46	6.06	3.38	6.54	7.33	7.79
MnO	0.06	0.04	0.11	0.24	0.21	0.23	0.03	0.04	0.13	0.11	0.11	0.10	0.08	0.11	0.11	0.03	0.02	0.03	0.02	0.11	0.04
P_2O_5	0.24	0.23	0.23	0.34	0.45	0.40	0.06	0.13	0.13	0.11	0.11	0.13	0.13	0.13	0.12	0.21	0.30	0.22	0.09	0.12	0.13
TiO_2	0.58	0.68	0.55	0.78	0.78	0.73	0.21	0.31	0.50	0.47	0.48	0.51	0.52	0.53	0.51	0.66	0.71	0.65	0.56	0.52	0.52
LOI	2.61	3.10	2.72	3.10	3.26	2.48	2.97	1.82	1.66	2.55	1.31	1.81	2.52	2.53	2.90	3.06	2.26	2.50	2.02	1.60	1.65
Total	99.9	99.8	99.8	99.9	99.7	100.2	101.0	99.9	99.9	101.1	99.9	100.0	99.8	100.3	100.5	99.8	99.0	100.2	99.8	99.0	99.9
Trace elements (ppm)																					
Li	8.84	18.0	33.8	9.81	17.4	20.0	34.4	9.90	58.5	28.6	31.9	36.0	37.4	40.9	42.3	9.41	22.9	6.14	8.45	19.4	34.0
Be	1.41	0.85	0.92	1.56	2.08	2.08	1.64	2.15	4.81	5.12	4.68	5.69	5.14	6.26	5.39	1.23	0.92	1.45	1.95	6.72	5.07
Sc	17.4	17.5	14.9	17.3	15.6	14.9	4.03	4.80	2.04	1.81	1.63	2.18	1.96	2.44	2.16	11.9	13.1	18.3	11.9	2.06	2.08
V	139	168	129	150	159	154	24.2	58.9	64.6	59.4	63.2	63.0	58.4	70.1	62.0	135	167	139	116	68.8	66.0
Cr	78.1	99.7	90.0	11.0	11.5	6.04	8.89	19.1	2.94	11.7	2.72	2.64	1.83	2.76	2.33	15.3	31.0	25.1	13.1	11.4	2.53
Co	12.5	13.4	12.0	16.7	20.0	21.9	5.05	3.81	4.01	2.92	3.21	3.61	2.96	4.14	3.45	13.1	5.94	12.3	5.55	3.37	1.58
Ni	21.0	22.0	22.2	21.8	14.2	8.79	10.9	14.2	8.33	7.93	7.12	7.74	8.75	11.5	9.77	19.1	11.7	18.1	7.45	6.43	5.17
Cu	420	742	375	11.7	4.78	5.37	3.00	2.54	11.5	7.13	8.67	12.9	10.7	10.6	12.6	38.3	4.64	6.84	88.6	6.01	9.75
Zn	311	432	226	127	55.9	57.0	11.0	23.8	95.7	89.0	91.8	88.3	81.8	97.2	131	17.9	30.7	34.0	41.2	111	96.8
Ga	18.5	20.7	16.8	19.6	24.3	21.6	16.6	18.4	25.0	23.5	23.7	22.9	22.4	24.8	22.6	17.1	12.0	18.2	16.9	24.2	24.8
Mo	2.64	1.45	1.33	1.08	1.19	0.757	1.28	1.25	3.28	2.85	3.06	1.41	1.69	0.99	1.68	3.83	1.55	4.18	19.2	1.83	1.52
Cd	0.62	0.55	0.59	0.10	0.03	0.07	0.05	0.05	0.12	0.10	0.13	0.11	0.27	0.14	0.18	0.05	0.04	0.03	0.13	0.13	0.11
Sb	8.97	4.19	7.84	1.23	0.44	0.55	0.39	0.24	0.74	0.65	0.63	0.65	0.85	0.59	0.62	0.22	0.48	0.29	1.31	0.53	0.53
W	7.03	2.66	8.99	0.83	0.60	0.57	0.79	0.53	4.01	3.26	3.17	2.26	2.48	2.15	2.41	1.21	4.57	1.40	2.66	2.14	2.02
Tl	1.53	1.41	1.53	1.72	1.08	1.02	0.12	0.69	1.17	1.04	1.08	1.15	1.29	1.09	0.92	0.42	0.36	0.25	0.73	1.36	1.35
Bi	0.37	0.22	0.86	0.06	0.05	0.03	0.05	0.11	0.44	0.45	0.44	0.46	0.47	0.46	0.45	0.15	0.26	0.13	1.08	0.36	0.45
Cs	1.63	2.07	5.02	3.14	7.57	6.42	1.68	1.70	77.30	7.40	7.71	12.20	5.03	12.1	10.9	6.24	2.44	4.89	2.59	2.56	2.64
Rb	237	174	217	176	114	108	23.2	147	176	159	170	168	175	166	150	105	95.8	59.2	145	179	182
Ba	2103	2656	2993	4107	608	602	96.9	649	746	766	693	809	668	822	776	395	1326	202	715	692	665
Th	5.43	5.41	5.24	9.72	4.25	3.44	13.6	25.2	27.9	24.3	24.5	23.7	25.7	26.3	24.7	10.9	8.46	11.0	9.54	27.6	27.3
U	1.94	2.03	1.98	2.59	1.23	1.11	4.73	3.57	7.51	5.81	6.36	5.80	4.76	5.21	6.45	4.95	3.02	4.84	4.20	6.31	7.57
Nb	5.27	5.81	4.90	9.07	7.14	5.80	15.8	12.7	23.0	21.7	21.7	21.7	21.7	22.9	21.1	6.19	8.81	7.31	9.70	23.7	23.9
Ta	0.37	0.35	0.33	0.55	0.37	0.35	1.28	1.16	1.21	1.18	1.22	1.17	1.22	1.24	1.17	0.56	0.65	0.65	0.60	1.32	1.35
La	16.6	10.8	15.1	21.3	11.8	11.9	45.2	29.1	121	122	118	118	101	120	118	24.0	33.7	40.2	30.9	127	127
Ce	39.1	21.5	30.3	53.8	26.7	26.3	82.8	60.9	235	223	232	223	229	238	227	41.7	62.2	62.8	61.3	245	244
Pb	222	235	85.3	20.6	5.21	4.54	2.56	4.49	27.3	23.1	26.6	24.4	37.9	26.1	36.8	3.20	10.8	5.91	31.9	53.7	66.4
Pr	4.04	2.71	3.92	5.66	3.67	3.54	9.43	7.37	29.1	30.4	28.8	27.8	23.4	29.5	28.1	4.82	7.83	6.80	8.01	30.6	30.8

Table 1. (continued)

Formation	Longwangshan						Dawangshan					Niangniangshan									
Sample No.	L1	L2	L3	L4	L5	L7	D10	D11	D22	D23	D25	N12	N13	N14	N15	N16	N17	N18	N19	N20	N21
Sr	69.3	115	57.4	164	439	280	71.7	198	2627	710	575	663	583	660	654	3149	716	339	329	554	548
Nd	17.0	12.2	17.5	24.5	17.5	16.5	35.5	27.9	114	123	119	112	92.3	120	113	19.6	35.7	27.1	31.2	123	122
Zr	133	143	127	226	196	160	137	128	633	444	444	432	456	496	450	99.8	101	103	112	654	631
Hf	3.66	3.69	3.37	6.11	4.93	3.97	4.69	4.08	13.2	10.5	10.6	10.2	10.8	11.3	10.4	2.98	3.10	3.08	3.18	13.7	13.4
Sm	3.36	2.43	3.50	5.10	4.40	3.78	7.16	4.98	21.3	22.5	21.2	21.0	17.2	21.8	21.5	3.89	7.82	4.86	5.63	22.6	21.9
Eu	0.89	0.61	0.98	1.78	1.60	1.12	0.924	1.20	4.85	5.34	5.13	4.72	3.86	5.12	4.75	1.32	1.72	1.61	1.68	4.88	4.98
Gd	2.68	2.17	3.06	4.49	3.86	3.48	5.53	3.84	15.3	16.1	15.7	15.1	12.4	15.4	15.5	3.32	5.73	4.15	4.12	15.7	15.8
Tb	0.47	0.42	0.54	0.79	0.70	0.64	0.95	0.60	2.20	2.34	2.27	2.10	1.81	2.30	2.19	0.55	0.98	0.67	0.62	2.31	2.24
Dy	2.43	2.22	2.94	3.83	3.85	3.43	5.18	3.11	9.63	10.1	9.70	9.01	8.60	10.4	9.15	2.86	5.55	3.73	3.19	10.1	9.78
Y	13.8	14.0	17.2	21.7	20.6	18.8	30.8	17.8	44.0	44.0	43.5	40.7	37.7	44.1	41.5	16.1	28.2	19.6	15.2	46.5	44.6
Ho	0.49	0.47	0.56	0.75	0.70	0.67	1.01	0.57	1.49	1.51	1.47	1.40	1.35	1.47	1.40	0.57	1.01	0.69	0.54	1.49	1.58
Er	1.59	1.66	1.91	2.44	2.17	2.13	3.31	1.89	4.16	4.26	4.22	4.10	3.80	3.99	3.94	1.75	3.29	2.24	1.66	4.33	4.21
Tm	0.25	0.32	0.31	0.37	0.33	0.33	0.57	0.29	0.59	0.56	0.55	0.56	0.50	0.56	0.58	0.29	0.49	0.35	0.25	0.59	0.58
Yb	1.71	1.74	2.01	2.61	2.13	2.15	3.86	1.94	3.52	3.34	3.29	3.24	3.11	3.45	3.16	1.84	3.13	2.18	1.80	3.53	3.59
Lu	0.26	0.26	0.31	0.41	0.36	0.35	0.61	0.31	0.51	0.46	0.45	0.41	0.42	0.48	0.47	0.28	0.45	0.34	0.32	0.53	0.53
ΣREE	90.9	59.5	82.9	128	79.8	76.3	202	144	563	565	562	542	499	572	549	107	170	158	151	592	589

reference zircons Plešovice (337 Ma) [*Sláma et al.*, 2008] and Qinghu (159 Ma) [*Li et al.*, 2009], and were polished. Cathodoluminescence (CL) images were obtained using a CAMECA SX50 microprobe at the Institute of Geology and Geophysics (IGG), Chinese Academy of Sciences, to identify the internal textures of zircons and to choose potential target sites for analyses. The mounts were coated with high-purity gold for ion-probe analysis. U-Pb dating of zircons was performed using a Cameca IMS-1280 ion microprobe at the IGG. Analytical procedures and data processing were the same as those described by *Li et al.* [2010]. During the measurements, oxygen flooding was used to increase the O_2 pressure to ~5×10^{-6} Torr in the sample chamber, enhancing the secondary Pb^+ sensitivity to a value of ~26 cps/nA/ppm for zircon. Pb/U calibration was performed relative to standard zircon 91500. Analyses of the standard zircon were interspersed with unknown grains. A long-term uncertainty of 1.5% (1 relative standard deviation, RSD) for $^{206}Pb/^{238}U$ measurements of the standard zircons was propagated to the unknowns, despite that the measured $^{206}Pb/^{238}U$ error in a specific session is generally around 1% (1 RSD) or less. To monitor the external uncertainties of SIMS U-Pb measurements calibrated against 91500 standard, Plešovice and Qinghu zircon standards were alternately analyzed together with the unknown zircons. The concordia ages of Plešovice and Qinghu zircons are 160.7 ± 1.5 Ma (2 system error, SE) and 335.5 ± 2.1 Ma (2 SE), respectively, which are identical with error with the recommended values of 159.45 ± 0.16 Ma [*Li et al.*, 2009] and 337.13 ± 0.37 Ma by TIMS [*Sláma et al.*, 2008]. In situ zircon Hf isotopic analyses were conducted using a Neptune MC-ICPMS with an ArF excimer laser ablation system at the IGG. Details of the analyses are given in *Zhang et al.* [2011].

[10] Chips of whole rock samples free of any weathered surface were crushed and ground in an agate mill to ~200 mesh. Major oxides and trace-element abundances were analyzed with an X-ray fluorescence spectrometer XRF-1500 and an ICP-MS ELEMENT at the IGG, respectively. The analytical precisions for all major and trace elements were better than 5% and accuracy was better than 5% for most elements by analyses of the GSR-3 standard [*Tang et al.*, 2006]. Sr, Nd, and Pb isotopic compositions of whole-rock powder were measured on a Finnigan MAT-262 thermal ionization mass spectrometer at the IGG. Repeat analyses yielded $^{87}Sr/^{86}Sr$ of 0.710255 ± 10 for the NBS-987 standard, $^{143}Nd/^{144}Nd$ of 0.511863 ± 9 for the La Jolla standard, $^{206}Pb/^{204}Pb$ of 16.917 ± 9,

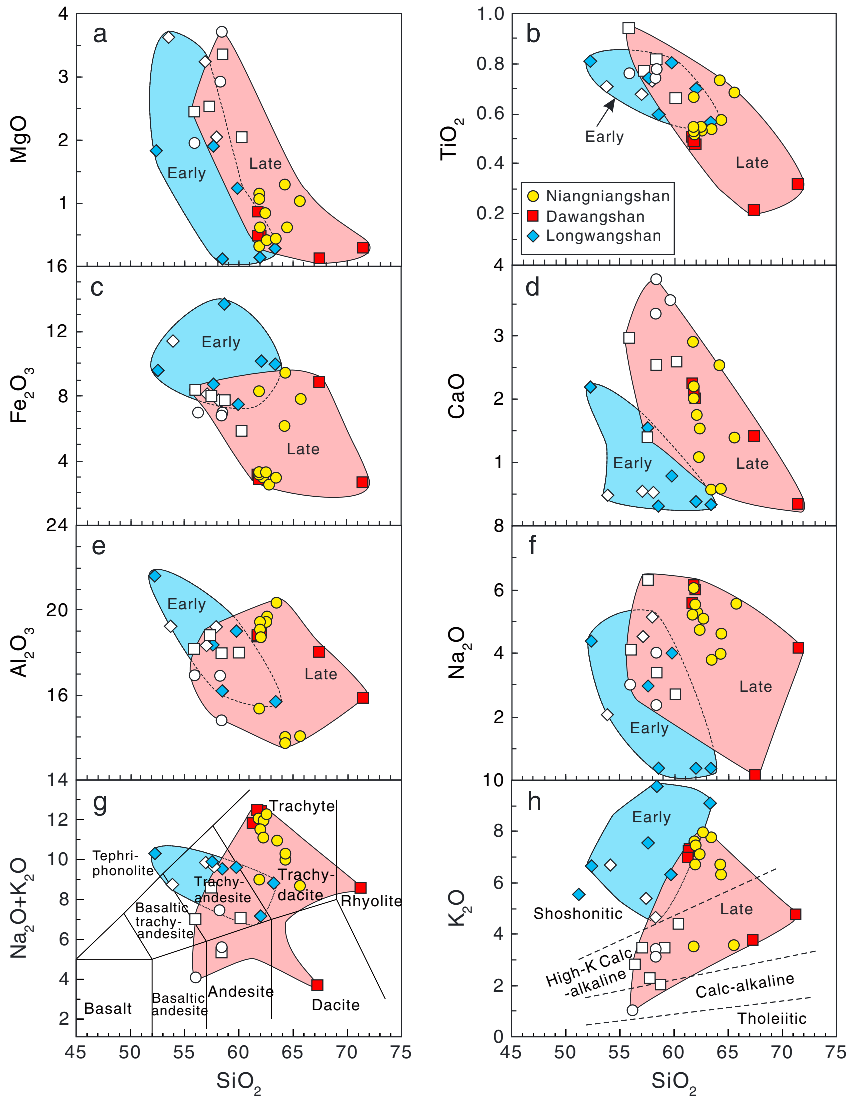

Figure 3. Major oxides plots for the Ningwu lavas. Open symbols represent published data [*Wang et al.*, 2001].

$^{207}Pb/^{204}Pb$ of 15.461 ± 10 and $^{208}Pb/^{204}Pb$ of 36.616 ± 12 for the NBS981 standard. Detailed descriptions of the techniques were given in *Tang et al*. [2006].

5. Results

5.1. Zircon Characteristics and U-Pb Data

[11] Most zircons are euhedral or subhedral, transparent, colorless and 100–300 μm in length with aspect ratios ranging from 2:1 to 4:1. Concentric zoning is common in most crystals under CL (Figure 2). The U-Pb analytical results are listed in Supporting Information[1] 2013GC004638-ts01. Uranium and Th concentrations vary widely, ranging from 51 to 860 ppm and from 28 to 1634 ppm, respectively. Th/U ratios vary in the range of 0.35 to 3.63. All analyses yield concordant ages of $^{206}Pb/^{238}U$ and $^{207}Pb/^{235}Pb$ within analytical error (Figure 2), demonstrating the U-Pb system of these zircons were closed since crystallization and did not experience loss or addition of U and Pb. The analytical data yield concordia ages of 133.3 ± 1.1 Ma (mean square of weighted deviates, MSWD = 0.01, 95% confidence level; same hereinafter) for the Longwangshan Formation, 131.0 ± 1.0 Ma (MSWD = 0.03) and 130.2 ± 1.1 Ma (MSWD = 0.53) for the Dawangshan Formation, and 130.4 ± 1.0 Ma (MSWD = 1.8) and 130.1 ± 1.0 Ma (MSWD = 1.0) for the Niangniangshan Formation. These ages can be interpreted as the best estimate of the crystallization age for the volcanic rocks. Based on the U-Pb ages, the Ningwu volcanic rocks

[1]Additional supporting information may be found in the online version of this article.

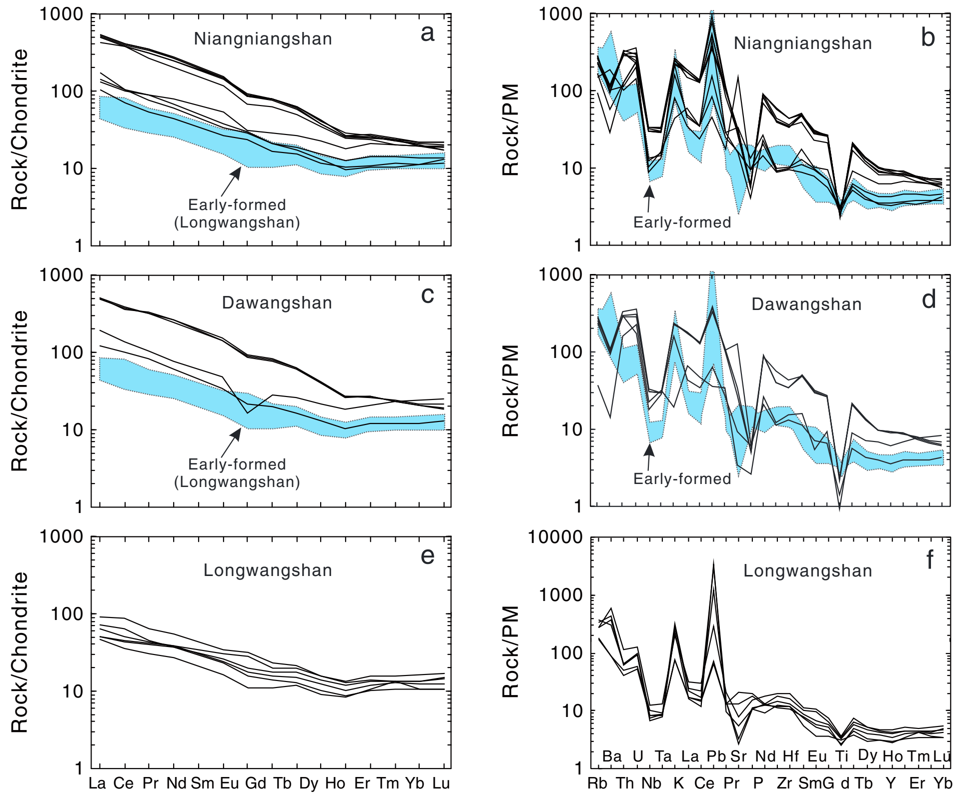

Figure 4. Chondrite-normalized rare earth element patterns and primitive mantle-normalized spider diagrams for the Ningwu lavas. The normalization values of Chondrite and primitive mantle are from *Anders and Grevesse* [1989] and *McDonough and Sun* [1995], respectively.

can be divided into two groups: early-formed lavas (~ 133 Ma) and late-formed lavas (~ 130 Ma).

5.2. Major and Trace Elements

[12] Major and trace element data are shown in Table 1. These rocks are dominantly shoshonitic and high-K calc-alkaline and range from trachyandesites to trachytes, with a few tephri-phonolite and dacite (Figure 3). They show large variations in major oxides (SiO_2 = 52–70%, Fe_2O_3 = 2.5–14%, Al_2O_3 = 14–22%, K_2O = 2.0–9.6%, Na_2O = 0.1–6.0%) and low MgO content (<4%). Plots of SiO_2 against major oxides show broadly negative correlations with MgO and TiO_2 (Figure 3). Most of the early-formed rocks have higher K_2O, Fe_2O_3 and TiO_2, lower SiO_2, CaO, and Na_2O contents than the late lavas, possibly reflecting fractional crystallization of olivine, clinopyroxene and feldspar in the evolution of these lavas.

[13] The Ningwu lavas show light rare earth element (LREE) enrichment in spite of some differences in their LREE/HREE fractionation (Figure 4). Some of them show slightly negative Eu anomalies, suggesting fractionation of a small amount of hornblende and/or feldspar. The absence of clear Eu anomalies in most of the lavas indicates no significant hornblende or feldspar crystallization. The late lavas have highly variable and higher REE contents (ΣREE = 107–589) than the early lavas (ΣREE = 76–128).

[14] In primitive mantle-normalized diagrams (Figure 4), the rocks show depletions in high field strength elements (HFSE) Nb, Ta, and Ti, but enrichment in K and Pb. The early lavas also show enrichment in large ion lithophile elements (LILE), Rb, and Ba, but depletion in Sr, except one sample with positive Sr anomaly. The most striking feature of the early lavas is highly enriched in Pb. The late lavas show negative P anomaly and positive Rb, Th, U, and Sr anomalies, except two samples with negative Sr anomaly.

5.3. Sr-Nd-Pb Isotopic Compositions

[15] The Sr-Nd and Pb isotopic compositions of the Ningwu lavas (Tables 2 and 3) show a negative correlation between $\varepsilon_{Nd}(t)$ and initial $^{87}Sr/^{86}Sr$ ratios and a linear array in $^{207}Pb/^{204}Pb$ vs. $^{206}Pb/^{204}Pb$ (Figure 5), generally parallel to the Northern Hemisphere Reference Line [*Zindler and Hart*, 1986]. The early

Table 2. Sr and Nd Isotopic Compositions of Volcanic Rocks From the Ningwu Basin[a]

Sample	^{87}Rb/^{86}Sr	^{87}Sr/^{86}Sr	2σ	(^{87}Sr/^{86}Sr)i	$\varepsilon_{Sr}(t)$	^{147}Sm/^{144}Nd	^{143}Nd/^{144}Nd	2σ	(^{143}Nd/^{144}Nd)i	$\varepsilon_{Nd}(t)$
L1	9.9938	0.724330	0.000010	0.705864	21.6	0.1170	0.512355	0.000011	0.512255	−4.2
L2	4.2541	0.713505	0.000008	0.705645	18.5	0.1210	0.512436	0.000007	0.512333	−2.7
L3	11.025	0.726771	0.000012	0.706400	29.2	0.1184	0.512380	0.000008	0.512279	−3.7
L4	3.1190	0.712760	0.000009	0.706997	37.7	0.1267	0.512294	0.000006	0.512186	−5.6
L5	0.6834	0.706323	0.000006	0.705060	10.2	0.1417	0.512366	0.000014	0.512246	−4.4
L7	1.0597	0.706983	0.00001	0.705020	9.7	0.1356	0.51237	0.000007	0.512255	−4.2
D11	2.1130	0.710302	0.000013	0.706398	29.2	0.0993	0.512289	0.000007	0.512205	−5.2
D22	0.1661	0.706443	0.000010	0.706136	25.5	0.1051	0.512401	0.000004	0.512312	−3.1
D23	0.9667	0.707244	0.000013	0.705463	15.8	0.1059	0.512400	0.000004	0.512310	−3.1
D25	0.8421	0.707251	0.000012	0.705695	19.2	0.1065	0.512390	0.000005	0.512299	−3.3
N12	0.6422	0.706991	0.000008	0.705804	20.7	0.1067	0.512384	0.000004	0.512293	−3.5
N13	0.7386	0.707295	0.000011	0.705930	22.5	0.1066	0.512378	0.000007	0.512287	−3.6
N14	0.6024	0.706996	0.000011	0.705883	21.9	0.1067	0.512380	0.000006	0.512289	−3.5
N15	0.5636	0.706844	0.000011	0.705803	20.7	0.1062	0.512385	0.000006	0.512295	−3.4
N16	0.0874	0.706863	0.000010	0.706702	33.5	0.1158	0.512262	0.000005	0.512164	−6.0
N17	0.312	0.707092	0.000007	0.706520	30.8	0.1246	0.512281	0.000007	0.512175	−5.8
N18	0.465	0.707106	0.000006	0.706250	27.0	0.1075	0.512268	0.000011	0.512177	−5.7
N19	1.2177	0.708525	0.000009	0.706275	27.4	0.1052	0.512368	0.000008	0.512279	−3.7
N20	1.0226	0.707392	0.000008	0.705503	16.5	0.1058	0.512467	0.000012	0.512377	−1.8
N21	0.8560	0.707413	0.000010	0.705831	21.1	0.1048	0.512396	0.000006	0.512307	−3.2

[a]Notation: Both $\varepsilon_{Sr}(t)$ and $\varepsilon_{Nd}(t)$ were obtained by assuming 130 Ma for the rocks.

lavas have highly variable (^{87}Sr/^{86}Sr)$_i$ (0.7050–0.7085) and high (^{207}Pb/^{204}Pb)$_i$ (up to 15.6) and (^{208}Pb/^{204}Pb)$_i$ (up to 38.4). In contrast, the late lavas have slightly lower Sr and Pb isotopic ratios. The isotopic compositions of the Ningwu lavas show similarities to those of marine sediments (Figure 5).

5.4. Zircon Hf Isotopic Compositions

[16] Zircons from the Ningwu lavas have variable Hf isotopic compositions with ^{176}Hf/^{177}Hf ratios from 0.2824 to 0.2827, corresponding to $\varepsilon_{Hf}(t)$ of +1.8 to −10 (Figure 5d; Supporting Information). The zircons from the early lavas have a smaller range of $\varepsilon_{Hf}(t)$ (+0.6 to −4.1) than those from the late lavas (+1.8 to −10). Both the lowest and highest $\varepsilon_{Hf}(t)$ values are observed in the late lavas.

6. Discussion

6.1. Geochronological Framework

[17] Early studies, based on K-Ar dating and Rb-Sr isochron, reported a wide range of ages (136 to 91 Ma) for the Ningwu volcanic rocks [*Yan et al.*, 2009, and references therein]. Subsequent studies reported zircon U-Pb ages by SHRIMP or LA-ICPMS for these rocks ranging from 131 ± 4 Ma to 127 ± 3 Ma [*Zhang et al.*, 2003a; *Yan et al.*, 2009; *Hou and Yuan*, 2010]. Thus, the time frame for the late lavas is clearly different. *Yan et al.* [2009] reported variable ages of the Niangniangshan Formation, from 128 ± 3 to 133 ± 3 Ma. However, recent zircon U-Pb dating work reported ages of 134.8, 132.2, 129.5, and 126.6 Ma for the Longwangshan, Dawangshan, Gushan, and Niangniangshan Formations, respectively [*Zhou et al.*, 2011]. The differences in the age data could be related to the samples because different authors sampled different flows. Moreover, most of the data have large errors (± 4 Ma) arising from the limitation of analytical technique. Given the analytical errors, these data indicate ages ranging from 135 to 127 Ma for the Ningwu lavas. In contrast, our age data for the magmatic zircons from the Ningwu lavas show 133 ± 1.1 Ma for the bottom layer of early lavas and 130.1 ± 1.0 Ma for the top layer of late-formed lavas (Figures 1 and 2). These high-precision age data, obtained by a new generation of large radius magnetic sector multicollector Cameca IMS-1280 ion microprobe using oxygen flooding techniques, indicate that there is no large time interval between the early and late volcanic activities in the Ningwu basin, and that these lavas formed in the Early Cretaceous and erupted rapidly within a short duration of ~ 3 Ma. The narrow window of eruption could be a response to rapid change of regional tectonic regime from extension to transpression caused by an inferred change in the direction of Pacific-Eurasia convergence (see section 6.3.1).

6.2. Petrogenesis

[18] The Early Cretaceous lavas from the Ningwu basin are characterized by enrichment in LREEs, K, and Pb, depletions in Nb, Ta, and Ti (Figure 4). These

Table 3. Pb Isotopic Compositions of the Ningwu Volcanic Rocks[a]

Sample	$^{206}Pb/^{204}Pb$	$^{207}Pb/^{204}Pb$	$^{208}Pb/^{204}Pb$	$^{204}Pb\%$	$^{238}U/^{204}Pb$	$^{235}U/^{204}Pb$	$^{232}Th/^{204}Pb$	$(^{206}Pb/^{204}Pb)_i$	$(^{207}Pb/^{204}Pb)_i$	$(^{208}Pb/^{204}Pb)_i$
L1	18.266	15.610	38.450	1.342	0.563	0.004	1.628	18.255	15.609	38.439
L2	18.251	15.596	38.401	1.344	0.556	0.004	1.530	18.240	15.595	38.391
L3	18.276	15.599	38.430	1.343	1.494	0.011	4.086	18.246	15.598	38.404
L4	18.379	15.589	38.512	1.340	8.114	0.059	31.462	18.214	15.581	38.309
L5	18.592	15.598	38.698	1.332	15.320	0.111	54.695	18.280	15.583	38.345
L7	18.564	15.598	38.676	1.333	15.855	0.115	50.769	18.241	15.582	38.348
D10	21.099	15.702	40.406	1.259	126.89	0.920	376.98	18.514	15.576	37.974
D11	20.047	15.663	40.443	1.276	53.873	0.391	392.93	18.950	15.610	37.908
D22	18.139	15.497	38.240	1.351	17.607	0.128	67.585	17.780	15.480	37.804
D23	18.088	15.492	38.197	1.353	16.076	0.117	69.473	17.761	15.476	37.749
D25	18.102	15.502	38.194	1.352	15.287	0.111	60.846	17.791	15.487	37.801
N12	18.100	15.487	38.205	1.352	15.196	0.110	64.161	17.790	15.472	37.791
N13	18.059	15.496	38.162	1.354	8.021	0.058	44.746	17.896	15.488	37.873
N14	18.104	15.492	38.210	1.352	12.764	0.093	66.575	17.844	15.479	37.780
N15	17.995	15.483	38.074	1.357	11.168	0.081	44.190	17.767	15.472	37.789
N16	20.385	15.663	39.705	1.283	104.26	0.756	237.22	18.261	15.560	38.174
N17	18.502	15.558	38.465	1.339	18.056	0.131	52.264	18.134	15.540	38.128
N18	19.161	15.606	38.892	1.319	53.695	0.389	126.09	18.067	15.553	38.078
N19	17.993	15.484	37.966	1.359	8.377	0.061	19.660	17.822	15.476	37.839
N20	18.022	15.510	38.110	1.355	7.496	0.054	33.881	17.869	15.503	37.891
N21	17.993	15.487	38.004	1.358	7.257	0.053	27.044	17.845	15.480	37.830

[a]Notation: Initial Pb isotope ratios were obtained by assuming 130 Ma for the rocks.

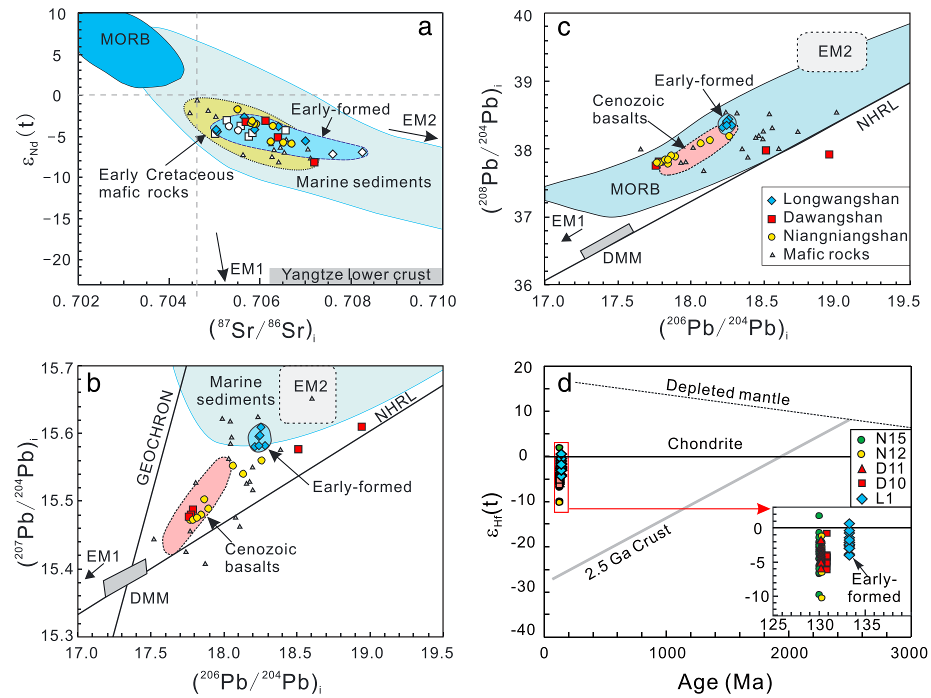

Figure 5. Plots of (a) $\varepsilon_{Nd}(t)$ vs. $(^{87}Sr/^{86}Sr)_i$, (b) $(^{207}Pb/^{204}Pb)_i$ and (c) $(^{208}Pb/^{204}Pb)_i$ vs. $(^{206}Pb/^{204}Pb)_i$, and (d) zircon $\varepsilon_{Hf}(t)$ vs. U-Pb ages for the Ningwu lavas. Data of the Early Cretaceous mafic rocks in the Lower Yangtze River region [*Yan et al.*, 2008] and fields for MORB, marine sediments [*Hofmann*, 2003] and Yangtze lower crust [*Jahn et al.*, 1999] are plotted for comparison. Other dada sources are as the same in Figure 3. The Northern Hemisphere reference line is after *Zindler and Hart* [1986].

geochemical signatures could result from three processes: (1) crustal contamination or assimilation and fractional crystallization (AFC), (2) partial melting of lower crust, and (3) partial melting of an enriched lithospheric mantle metasomatized by slab-derived fluid/melt [*Wang et al.*, 2006; *Yan et al.*, 2008].

6.2.1. Crustal Contamination?

[19] Mixing between mantle-derived magma and upper crustal material will generate a clearly negative correlation between Nd isotopic ratios and SiO_2 because upper crust has high SiO_2 contents and low $\varepsilon_{Nd}(t)$ values [*Jahn et al.*, 1999]. However, the $\varepsilon_{Nd}(t)$ values for the early lavas are nearly constant with increasing SiO_2 (Figure 6a), arguing against significant upper crustal contamination during magma ascent for the early lavas. In contrast, the very weak correlation between SiO_2 and $\varepsilon_{Nd}(t)$ for the late lavas suggests a very low-degree contamination, which is also evidenced in the AFC models of trace elements (Figures 6b–6d). Furthermore, the contents of K_2O (3.4–9.6%), Ba (up to 4107 ppm; Figure 6b) and Pb (up to 235 ppm; Table 1) of these lavas are much higher than those of upper continental crust (K_2O = 2.8%, Ba = 628 ppm, Pb = 17 ppm) and lower continental crust (K_2O = 0.6%, Ba = 259 ppm, Pb = 4 ppm) [*Rudnick and Gao*, 2003]. The Cr (most <20 ppm), Co (most <15 ppm) and Ni (most <22 ppm) contents of the rocks are much lower than those of upper continental crust (Cr = 92 ppm, Co = 17 ppm, Ni = 47 ppm) and lower continental crust (Cr = 215 ppm, Co = 38 ppm, Ni = 88 ppm) [*Rudnick and Gao*, 2003]. The low concentrations of Cr, Co and Ni could not have resulted from AFC, as this would result in progressive decrease in Cr, Co, Ni, and Mg# with concomitant increase in $^{87}Sr/^{86}Sr$ ratios and decrease in $^{143}Nd/^{144}Nd$ ratios. These features are not observed in our samples. Therefore, we infer that the Ningwu magmas did not experience significant crustal contamination during ascent through the crust. Thus, the compositional characteristics of these lavas can be used to probe their mantle sources.

6.2.2. Fractional Crystallization

[20] Most of the lavas with low and variable MgO, Ni, and Cr contents (Table 1) might have experienced fractional crystallization of olivine and pyroxene. This is consistent with the broadly negative correlations between MgO, TiO_2, CaO, and Al_2O_3 with SiO_2 (Figure 3). The models of fractional crystallization (Figure 7) further indicate

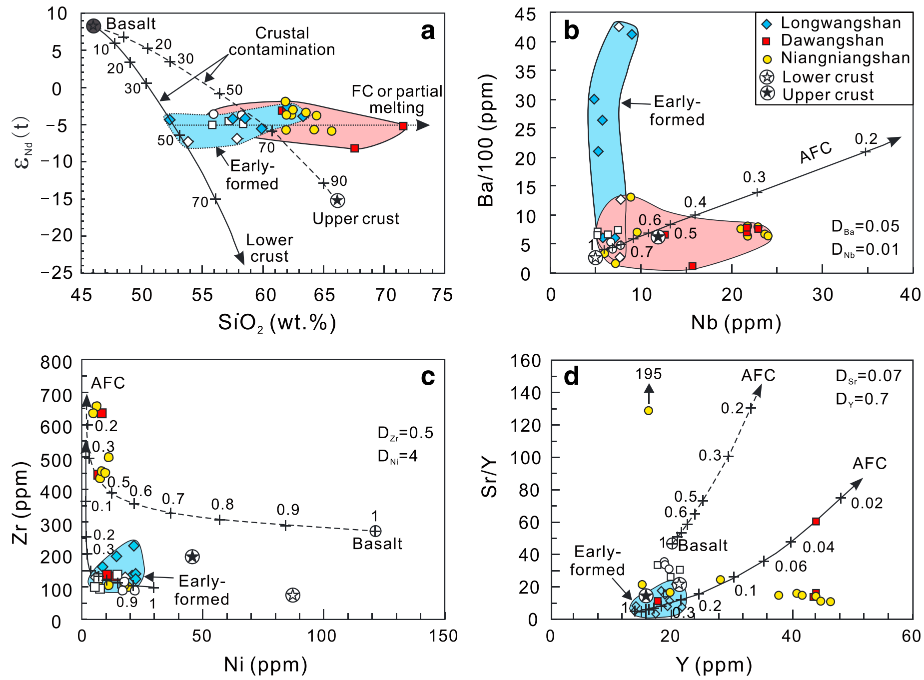

Figure 6. Plots of (a) SiO_2 vs. $\varepsilon_{Nd}(t)$, (b) Nb vs. Ba, (c) Ni vs. Zr, and (d) Y vs. Sr/Y for the Ningwu lavas, showing the possible role of crustal assimilation and fractional crystallization (AFC). The curves labeled with numbers in Figure 6a represent crustal contamination of mantle-derived melt, and the numbers indicate the percentage of the contribution of crustal components. In Figures 6b, 6c, and 6d, the solid and dashed curves represent AFC for hypothesized early magmas according to the Longwangshan lavas and continental basalts, respectively. The assimilation ratio is assumed to be 0.1. The numbers labeled on the curves are the amount of magma remaining. Data sources: bulk partition coefficients (*D*) [*Rollinson*, 1993], upper and lower continental crust [*Jahn et al.*, 1999; *Rudnick and Gao*, 2003], the basalt [*Tang et al.*, 2006]. Other dada sources and symbols are as the same in Figure 3.

significant crystallization of clinopyroxene, olivine, hornblende, biotite and K-feldspar. Slightly negative Eu and Sr anomalies in several samples (Figure 4) suggest a small amount of plagioclase fractionation. The lack of clear Eu and Sr anomalies in most of the lavas indicate that the fractional crystallization of plagioclase is insignificant. The negative P anomaly in the late lavas (Figure 4) implies the crystal fractionation of apatite. The distribution of the lavas in the plots of SiO_2 vs. $\varepsilon_{Nd}(t)$ (Figure 6a) and covariations between trace elements (Figure 7) indicate that the geochemical variations in the Ningwu lavas might have resulted mainly from fractional crystallization and/or partial melting, rather than crustal contamination.

6.2.3. Partial Melting of Lower Crust

[21] Most of the Ningwu lavas fall in the fields for adakitic rocks derived from partial melting of lower crust [*Wang et al.*, 2006] due to their low compatible element abundances (e.g., Ni), MgO contents and Mg# values (Figure 8). This indicates that these lavas could be derived from partial melting of lower crust. However, the very low MgO contents and Mg# in these lavas are also consistent with the results of melting experiments of natural, hydrous basalts at 1–4 GPa (Figures 8b and 8c), which suggest that these lavas could also be derived from partial melting of subducted oceanic slab. Many samples have higher MgO (> 3 wt %) contents and Mg# (>40) values than the pristine experimental melts [*Rapp et al.*, 1999], suggesting that they experienced different degrees of interaction with the mantle during ascent, a process by which silicic melts can dramatically elevate their MgO and Mg# (Figure 8c). Therefore, if the Ningwu lavas were derived from lower continental crust or subducted oceanic slab, some of them must have interacted with the mantle. Given that these rocks have highly radiogenic Pb isotopic ratios with $^{206}Pb/^{204}Pb_{(t)}$ of 17.8–19, evidently higher than those of adakites derived from partial melting of lower continental crust (<16.4) [*Liu et al.*, 2010], the magma genesis of the Ningwu lavas was likely related to subducted oceanic crust. This is also consistent with their highly radiogenic Sr isotopic ratios at a given $\varepsilon_{Nd}(t)$ (Figure 5a). Based on the above discussions, we infer that the Ningwu lavas were derived from partial melting of an enriched

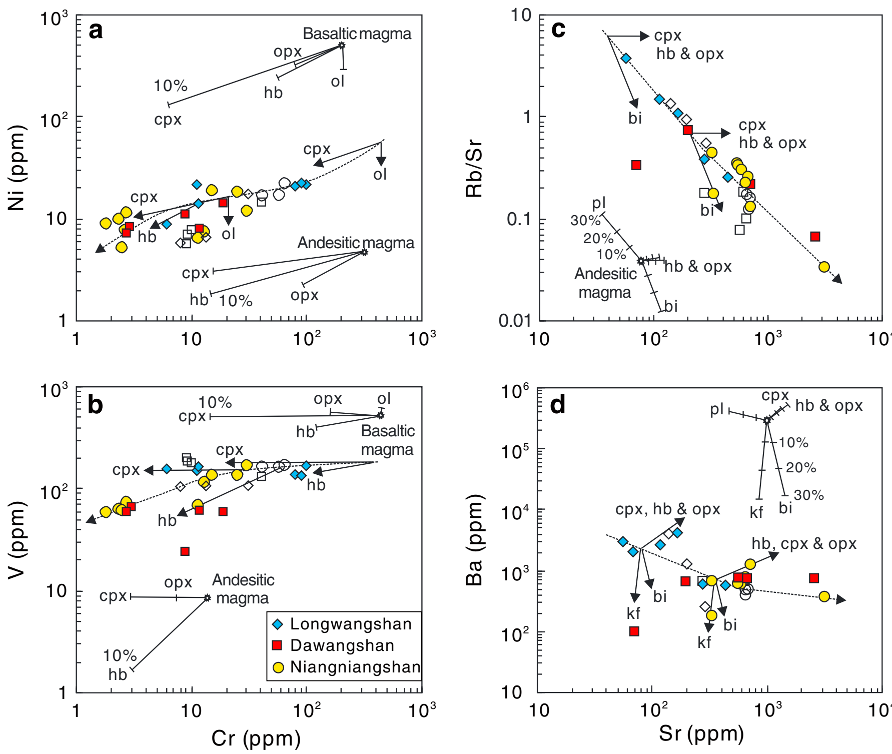

Figure 7. Plots of (a) Ni and (b) V vs. Cr, (c) Rb/Sr, and (d) Ba vs. Sr for the Ningwu lavas, showing the possible fractional crystallization of olivine (ol), clinopyroxene (cpx), orthopyroxene (opx), hornblende (hb), biotite (bi), and K-feldspar (kf). The models are from *Yang et al.* [2005]. Dada sources and symbols are as the same in Figure 3.

lithospheric mantle metasomatized by slab-derived fluid/melt (see below).

6.2.4. Enriched Lithospheric Mantle Metasomatized by Marine Sediments

[22] The major, trace element and Sr-Nd isotopic compositions suggest that the Ningwu volcanic rocks were possibly derived from enriched lithospheric mantle metasomatized by subducted oceanic sediments. This inference is also supported by the following lines of evidence.

[23] The Cretaceous mafic rocks from the Lower Yangtze River region have enriched Sr-Nd isotopic characteristics and highly radiogenic Pb isotopic compositions and were believed to be derived from enrich lithospheric mantle metasomatized by slab-derived material [*Yan et al.*, 2008]. The Ningwu lavas have geochemical signatures very similar to those of the Cretaceous mafic rocks (Figures 5a–5c and 9c), indicating that they could be also derived from a similar enriched mantle source. In the diagrams of Sr, Nd, and Pb isotopes (Figure 5), these rocks show a trend toward the EM-2 end-member, reflecting the important role of marine sediments in magma source. The early lavas have higher $(^{87}Sr/^{86}Sr)_i$ and $(^{207}Pb/^{204}Pb)_i$ values than the late, indicating greater involvement of marine sediments in the petrogenesis of the early lavas than the late.

[24] The zircons $\varepsilon_{Hf}(t)$ values (+1.8 to −10) of the lavas also suggest their derivation from an enriched lithospheric mantle. The larger $\varepsilon_{Hf}(t)$ variation in the late lavas could reflect low-degree magma mixing of metasomatized lithospheric mantle-derived melts with asthenospheric and siliceous crustal melts. The siliceous crustal melts might have formed as a result of underplating of mantle-derived magma in the lower crust, which triggered partial melting of the basement rocks (e.g., old mafic granulites and TTG gneisses [*Chen et al.*, 2013].

[25] In the plot of Nb/Yb vs. Th/Yb, the Ningwu lavas plot above the MORB-OIB array (Figure 9a), clearly suggesting a subduction-related component in their sources, i.e., interaction with fluid/melt released from a subducted slab results in high Th and low Nb in the upper mantle wedge [*Pearce et al.*, 1995]. La/Nb and Ba/Nb ratios in these rocks are higher than those of OIB, primitive mantle, N-MORB and average continental crust (Figure 9b), but similar to those of arc volcanic rocks. These ratios suggest the role of crustal materials (granulites,

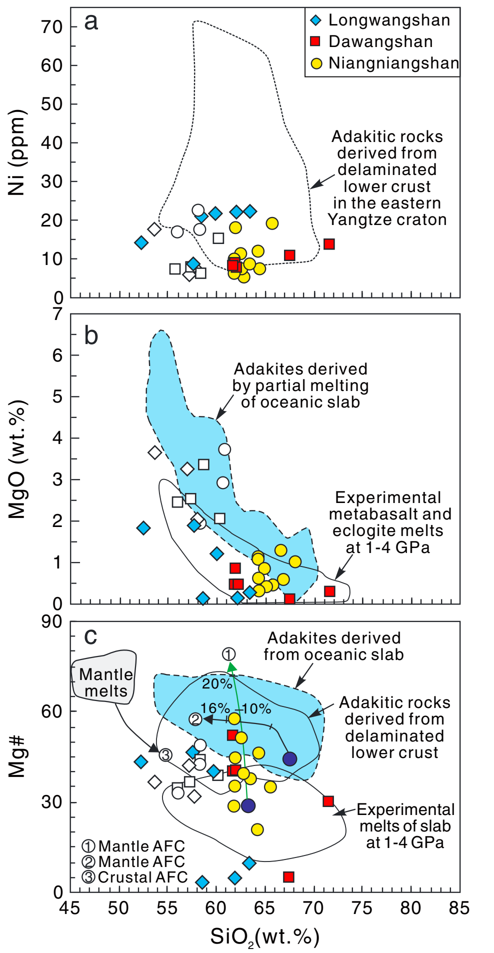

Figure 8. Plots of (a) Ni, (b) MgO, and (c) Mg# vs. SiO_2 for the Ningwu lavas. Data sources: fields for delaminated lower crust-derived adakitic rocks and subducted oceanic slab-derived adakites [*Wang et al.*, 2006], mantle AFC curve 1 and crustal AFC curve 3 [*Stern and Kilian*, 1996], field for experimental melts at 1–4 GPa and mantle AFC curve 2 [*Rapp et al.*, 1999]. Other data sources and symbols are as the same in Figure 3.

sediments, etc.) in the magma genesis of the lavas. The positive Pb anomaly (Figure 4) and high Pb/Ce ratios (Figure 9c) of the lavas also indicate their enriched mantle source metasomatized by subducted sediments [*Othman et al.*, 1989; *Wang et al.*, 2006].

[26] In summary, the geochemical characteristics of the Ningwu lavas are markedly similar to those of Cretaceous shoshonitic [*Wang et al.*, 2006] and mafic rocks [*Yan et al.*, 2008] in the neighboring areas. These features could be mainly derived from enriched lithospheric mantle metasomatized by fluids/melts from subducted sediments. The geochemical variations are largely attributed to the differential melting of a heterogeneous source. The early lavas likely had more contributions of subducted marine sediments in their magma genesis and were derived from higher degrees of partial melting than the late lavas (Figure 9d) because the subducted components are fusible and could melt early [*Xu et al.*, 2012]. Due to the consumption of a significant volume of fusible components in early phase of melting, the late lavas mostly originated from a mantle source with relatively less subducted components than that of the early lavas. Large variation in Nd and Hf isotopic compositions probably indicate greater involvement of melts from asthenosphere and lower crust during the magma genesis of the late-formed lavas.

6.3. Implications for Lithospheric Evolution of Eastern China

6.3.1. Change in Plate Convergence Direction

[27] It is generally agreed that the Pacific plate has been subducting southwestward beneath Eurasia since the Jurassic [cf. *Zhou and Li*, 2000; *Zhou et al.*, 2006]. Subduction direction of the Pacific plate was nearly parallel to the east boundary of the Eurasian continent before ca. 125 Ma (Figure 10). Such subduction has been interpreted to have driven roughly south-northward extension and extension-related magmatism in the Eurasian upper plate during the Early Cretaceous [*Sun et al.*, 2007, and references therein]. Sometime in the Early Cretaceous, the direction of plate convergence appears to have changed by ~80° from roughly southward to northwestward subduction (Figure 10) [*Koppers et al.*, 2001; *Sun et al.*, 2007, and references therein]. The change in convergence direction coincides with a change from extension to transpression in eastern China as evidenced by the sinistral slip along the Tan-Lu fault zone [*Zhang et al.*, 2003b] and the cessation of the magmatism temporally related to the extensional setting [*Li*, 2000].

[28] The formation of the Ningwu lavas (ca. 133–130 Ma) coincides temporally with the tectonic switching from extension to a transpression in eastern China. In the Early Cretaceous, the thickened mountain root underneath the Dabie Orogen, which formed during the Triassic Yangtze-North China continental collision [*Li et al.*, 1993], collapsed due to gravitational instability and lithospheric extension [*Xu et al.*, 2007]. The effects of mountain-root collapse can explain the dramatic stress change, rapid eruption of the Ningwu lavas, and the Early Cretaceous large-scale magmatism in this region [*Liu et al.*, 2012 and references therein]. It has been suggested that the Cretaceous magmatism in

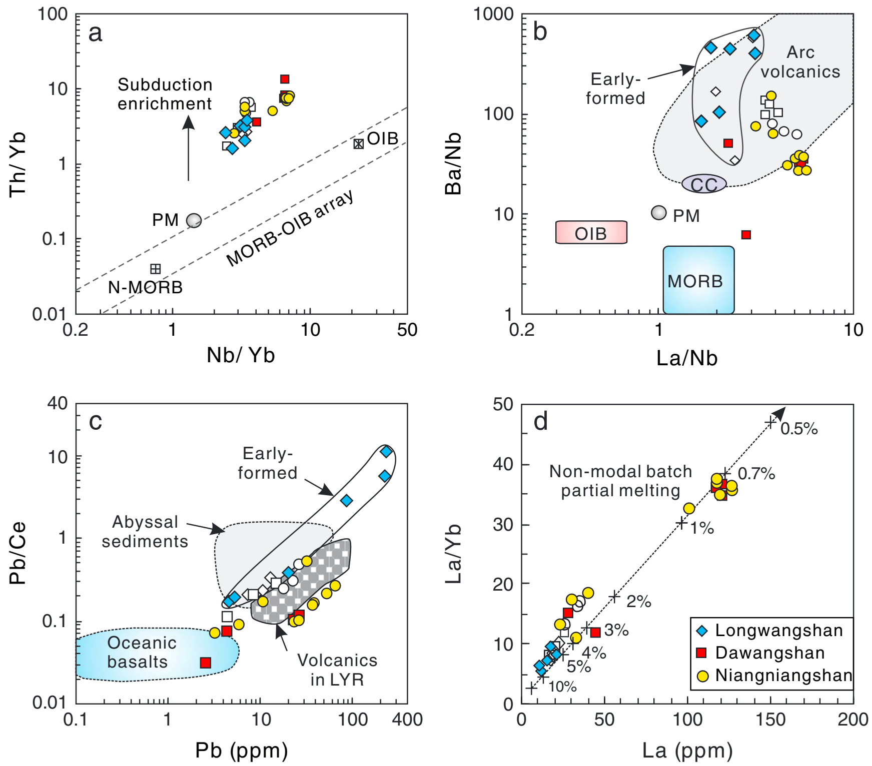

Figure 9. Variations of (a) Th/Yb vs. Nb/Yb, (b) La/Nb vs. Ba/Nb, (c) Pb vs. Pb/Ce, and (d) La vs. La/Yb for the Ningwu lavas. In the modeling of batch partial melting in Figure 9d, the assumed modes of ol, opx, cpx, spinel, garnet, and abundances of La and Yb in source peridotite are 56, 29, 5.5, 2, 7.5, and 1.32 and 1.18 ppm, respectively. The numbers labeled on the dashed line denote melting degrees. Data sources: partition coefficients and melt mode for modeling [*Tang et al.*, 2006], PM, N-MORB, and OIB [*Sun and McDonough*, 1989], MORB-OIB array [*Pearce and Peate*, 1995], continental crust (CC) [*Rudnick and Gao*, 2003], Oceanic basalts and abyssal sediments [*Othman et al.*, 1989], Arc volcanics [*Jahn et al.*, 1999], Cretaceous volcanic rocks in the Lower Yangtze River (LYR) region [*Wang et al.*, 2006], other dada sources and symbols as the same in Figure 3.

southeastern China be a response to regional extension setting associated with contemporary subduction of the Pacific plate [*Zhou et al.*, 2006; *Wang et al.*, 2006, and references therein]. The cessation of the extension-related volcanism at ca. 130 Ma coincides with the tectonic switching from extension to transpression in eastern China, i.e., the inferred change in the direction of Pacific plate subduction from roughly southward to northwestward. Thus, the narrow window of eruption of the Ningwu volcanic rocks likely signifies a rapid change in regional tectonic setting and the direction of Pacific-Eurasia convergence in the Early Cretaceous.

6.3.2. Lithospheric Evolution of Eastern China and Pacific Subduction

[29] Previous studies of peridotite xenoliths from kimberlites have indicated a thick (>200 km) lithosphere in eastern China prior to the Paleozoic, while basalt-borne xenoliths reveal the presence of thin (<80 km) lithosphere in the Cenozoic, which indicates large-scale thinning of the lithosphere (>120 km) and significant tectonothermal reactivation occurred in eastern China in the Mesozoic [*Menzies et al.*, 2007, and references therein]. These events were accompanied by the dramatic change in the physical and chemical properties of the lithospheric mantle (from old, cool and highly refractory to relatively young, hot and fertile), suggesting an intensive lithospheric modification and destruction via lithospheric removal and/or replacement/erosion of an ancient cratonic lithosphere by a juvenile oceanic-type lithosphere in eastern China [*Xu*, 2001; *Menzies et al.*, 2007; *Zhang et al.*, 2008]. The mechanism for lithospheric destruction has been a hot topic for more than 20 years. Zhang [2009] correlated the destruction processes to high mantle temperatures in the Early Cretaceous, lithospheric modification by addition of volatiles and lithospheric extension related to the subduction of circum-craton plates since the Paleozoic. The subduction and rollback of the Pacific plate during the Mesozoic has been proposed to be a

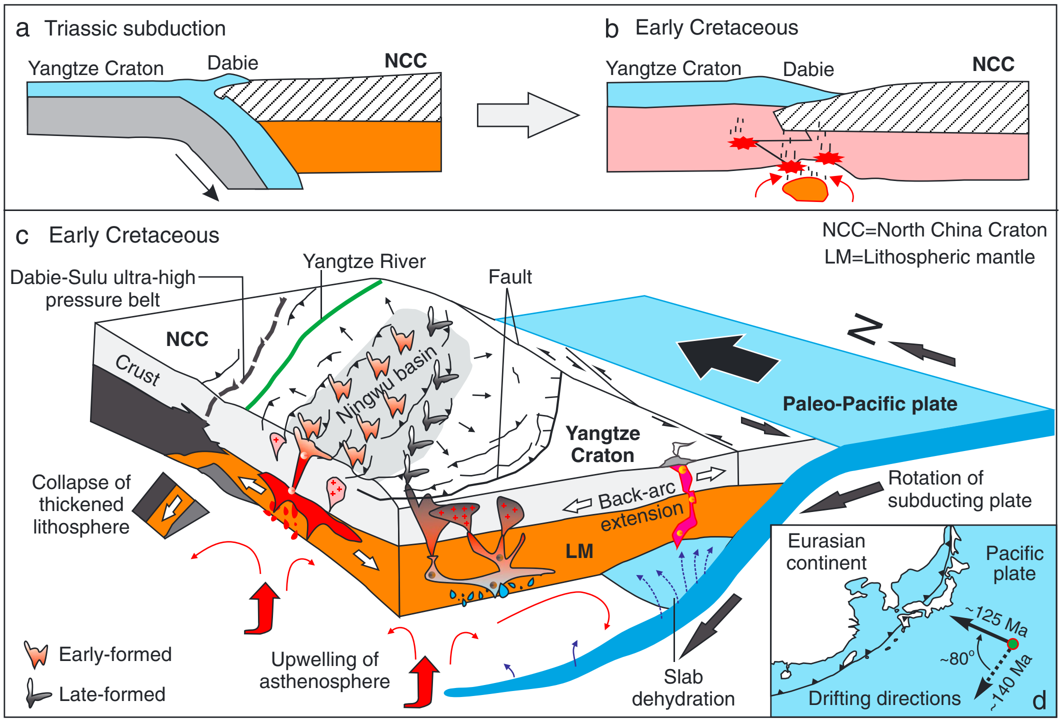

Figure 10. Schematic maps showing (a) Triassic collision between the Yangtze Craton and North China Craton, leading to the formation of Dabie Orogen, (b) Early Cretaceous collapse of the mountain root underneath Dabie Orogen, (c) combined effects of the distinct processes of formation of the Ningwu basin and the Cretaceous volcanic rocks (modified after *Meng* [2003] and *Zhao et al.* [2007]), and (d) change in the direction of Pacific plate subduction by ~80° from roughly southward to northwestward in the Early Cretaceous, modified after *Koppers et al.* [2001] and *Sun et al.* [2007]. Subduction of the Pacific plate and mountain-root collapse resulted in stretching and thinning of the Ningwu lithosphere and upwelling of the asthenosphere, which promoted mantle partial melting and voluminous magmatism. Considering the spatio-temporal relationship and geochemical signatures of the Ningwu lavas (the early lavas distributed along the eastern margin of the basin; Figure 1), the most probable explanation is that more fusible subducted components melted during the early-phase melting of mantle source and thus the early lavas bear stronger subduction-related signatures than the late lavas. The genesis of these rocks was mainly controlled by the subduction of Pacific plate and the plate interactions in eastern Eurasia.

crucial trigger that caused "back-arc" extension, thermo-mechanical and chemical erosion [*Zheng et al.*, 2007; *Zhang et al.*, 2009; *Zhu et al.*, 2012, and references therein] and/or delamination [*Gao et al.*, 2004] of the lithospheric mantle, finally leading to the destruction of the lithosphere [*Zhu et al.*, 2012; *Tang et al.*, 2013].

[30] The subduction of the Paleo-Pacific plate beneath eastern Eurasia likely provided the contribution of marine sediments, as recent studies show that a large volume of sediments are dragged down along with the subducting plate in convergent margins [*Kawai et al.*, 2013; *Ichikawa et al.*, 2013], which led to the enrichment of mantle source of the Cretaceous lavas in eastern China (Figure 10). The alternative possibility that the enriched mantle signature was generated during an earlier event, prior to the Pacific plate subduction, cannot be excluded. Considering the proximal oceanic plate subduction, we favor that the enriched mantle was metasomatized by the Pacific plate-derived material, which is also consistent with the fact that the Early Cretaceous adakites along the Lower Yangtze River region bear more affinity to oceanic crust than those on the southeastern North China Craton [*Liu et al.*, 2010].

7. Conclusions

[31] The volcanic rocks from the Ningwu basin in eastern China formed in the Early Cretaceous and erupted rapidly within a short duration (ca. 133–130 Ma). These lavas mostly belong to shoshonitic and high-K calc-alkaline series, and are characterized by enrichment in LREE, K, and Pb, depletions in HFSE, highly radiogenic Sr and Pb isotopic compositions and variable $\varepsilon_{Hf}(t)$ values (+1.8 to −10). These features suggest that

the lavas were mainly derived from an enriched lithospheric mantle metasomatized by subducted marine sediments. The early lavas show stronger signatures of marine sediments than the late lavas, indicating that the latter mainly originated from a mantle source with less subducted components than that of the former due to the consumption of a significant volume of the fusible components in the early phase of melting. Large $\varepsilon_{Hf}(t)$ variation in the late lavas suggests greater involvement of melts from asthenosphere and lower crust during their magma genesis.

[32] The formation of the Ningwu lavas coincides temporally with a regional tectonic switching from extension to transpression. The narrow window of eruption of the lavas may signify a rapid change in tectonic setting and plate convergence direction, i.e., the inferred change in the direction of Pacific plate subduction from roughly southward to northwestward. Subduction of the Pacific plate may have driven small-scale convective instabilities at the base of the overriding lithosphere, possibly resulting in gradual weakening and thinning of the lithosphere. The lithospheric evolution of eastern China is closely coupled with the subduction of the Pacific plate underneath eastern Eurasia.

Acknowledgments

[33] We greatly appreciate the thorough reviews and helpful comments from Cin-Ty Lee, Esteban Gazel and an anonymous reviewer, which helped to improve and clarify the presentation. We also thank the staffs of the State Key Laboratory of Lithospheric Evolution at the IGG, CAS, for assistance with zircon, element and isotopic analyses. This work was supported by the CAS (grant KZCX1-YW-15-2) and NSF grant 41073028. This study is also a contribution to the 1000 Talent Award to M. Santosh from the Chinese Government.

References

Anders, E., and N. Grevesse (1989), Abundances of the elements: meteoritic and solar, *Geochim. Cosmochim. Acta*, *53*, 197–214, doi:10.1016/0016-7037(89)90286-X.

Anderson, A. T. (1976), Magma mixing: petrological process and volcanological tool, *J. Volcano. Geotherm. Res.*, *1*, 3–33, doi:org/10.1016/0377-0273(76)90016-0.

Chen, B., B. M. Jahn, and K. Suzuki (2013), Petrological and Nd-Sr-Os isotopic constraints on the origin of high-Mg adakitic rocks from the North China Craton: Tectonic implications, *Geology*, *41*, 91–94, doi:10.1130/g33472.1.

Chen, J. F., J. Yan, Z. Xie, X. Xu, and F. Xing (2001), Nd and Sr isotopic compositions of igneous rocks from the Lower Yangtze region in eastern China: constraints on sources, *Phys. Chem. Earth (A)*, *26*, 719–731, doi:10.1016/S1464-1895(01)00122-3.

Gao, S., R. L. Rudnick, R. W. Carlson, W. F. McDonough, and Y. S. Liu (2002), Re-Os evidence for replacement of ancient mantle lithosphere beneath the North China craton, *Earth Planet. Sci. Lett.*, *198*, 307–322, doi:10.1016/S0012-821X(02)00489-2.

Gao, S., et al. (2004), Recycling lower continental crust in the North China craton, *Nature*, *432*, 892–897, doi:10.1038/nature03162.

Hofmann, A. W. (2003), Sampling mantle heterogeneity through oceanic basalts: isotope and tract elements, in *The Mantle and Core. Treatise on Geochemistry*, edited by R. W. Carlson, pp. 61–101, Elservier-Pergamon, Oxford.

Hou, K. J., and S. D. Yuan (2010), Zircon U-Pb age and Hf isotopic composition of the volcanic and sub-volcanic rocks in the Ningwu basin and their geological implications, *Acta Petro. Sin.*, *26*, 888–902, in Chinese with English abstract.

Ichikawa, H., M. Kameyama, and K. Kawai (2013) Mantle convention with continental drift and heat source around the mantle transition zone, Gondwana Research, doi:10.1016/j.gr.2013.02.001.

Jahn, B. M., F. Y. Wu, C. H. Lo, and C. H. Tsai (1999), Crust-mantle interaction induced by deep subduction of the continental crust: geochemical and Sr-Nd isotopic evidence from post-collisional mafic-ultramafic intrusions of the northern Dabie complex, central China, *Chem. Geol.*, *157*, 119–146, doi:10.1016/S0009-2541(98)00197-1.

Kawai, K., S. Yamamoto, T. Tsuchiya, and S. Maruyama (2013), The second continent: Existence of granitic continental materials around the bottom of the mantle transition zone, *Geosci. Front.*, *4*, 1–6, doi:10.1016/j.gsf.2012.08.003.

Koppers, A. A. P., J. P. Morgan, J. W. Morgan, and H. Staudigel (2001), Testing the fixed hotspot hypothesis using 40Ar/39Ar age progressions along seamount trails, *Earth Planet. Sci. Lett.*, *185*, 237–252, doi:10.1016/S0012-821X(00)00387-3.

Li, S. G., et al. (1993), Collision of the North China and Yangtze Blocks and formation of coesite-bearing eclogite-timing and processes, *Chem. Geol.*, *109*, 89–111, doi:10.1016/0009-2541(93)90063-O.

Li, X. H. (2000), Cretaceous magmatism and lithospheric extension in Southeast China, *J. Asian Earth Sci.*, *18*, 293–305, doi:10.1016/S1367-9120(99)00060-7.

Li, X. H., Y. Liu, Q. L. Li, and C. H. Guo (2009), Precise determination of Phanerozoic zircon Pb/Pb age by multicollector SIMS without external standardization, *Geochem. Geophy. Geosys.*, *10*, Q04010, doi:10.1029/2009GC002400.

Li, X. H., W. X. Li, X. C. Wang, Q. L. Li, Y. Liu, G. Q. Tang, Y. Y. Gao, and F. Y. Wu (2010), SIMS U-Pb zircon geochronology of porphyry Cu-Au-(Mo) deposits in the Yangtze River Metallogenic Belt, eastern China: Magmatic response to early Cretaceous lithospheric extension, *Lithos*, *119*, 427–438, doi:10.1016/j.lithos.2010.07.018.

Li, Z. X., and X. H. Li (2007), Formation of the 1300-km-wide intracontinental orogen and postorogenic magmatic province in Mesozoic South China: A flat-slab subduction model, *Geology*, *35*, 179–182, doi:10.1130/g23193a.1.

Liu, S. A., S. G. Li, Y. S. He, and F. Huang (2010), Geochemical contrasts between early Cretaceous ore-bearing and ore-barren high-Mg adakites in central-eastern China: Implications for petrogenesis and Cu-Au mineralization, *Geochim. Cosmochim. Acta*, *74*, 7160–7178, doi:10.1016/j.gca.2010.09.003.

Liu, S. A., S. Li, S. Guo, Z. Hou, and Y. He (2012), The Cretaceous adakitic-basaltic-granitic magma sequence on south-eastern margin of the North China Craton: Implications for lithospheric thinning mechanism, *Lithos*, *134–135*, 163–178, doi:10.1016/j.lithos.2011.12.015.

Mao, J., F. Pirajno, and N. Cook (2011), Mesozoic metallogeny in East China and corresponding geodynamic settings — An introduction to the special issue, *Ore Geol. Rev.*, *43*, 1–7, doi:10.1016/j.oregeorev.2011.09.003.

McDonough, W. F., and S. S. Sun (1995), The composition of the earth, *Chem. Geol.*, *120*, 223–253, doi:10.1016/0009-2541(94)00140-4.

Meng, Q. R. (2003), What drove late Mesozoic extension of tghe northern China-Mongolia tract, *Tectonophysics*, *369*, 155–174, doi:10.1016/S0040-1951(03)00195-1.

Menzies, M., Y. G. Xu, H. F. Zhang, and W. M. Fan (2007), Integration of geology, geophysics and geochemistry: A key to understanding the North China Craton, *Lithos*, *96*, 1–21, doi:10.1016/j.lithos.2006.09.008.

Othman, D. B., W. M. White, and J. Patchett (1989), Geochemistry of marine sediments, island arc magma genesis and crust-mantle recycling, *Earth Planet. Sci. Lett.*, *94*, 1–21, doi:10.1016/0012-821X(89)90079-4.

Pearce, J. A., and D. W. Peate (1995), Tectonic implications of the composition of volcanic arc magmas, *Annu. Rev. Earth Planet. Sci.*, *23*, 251–285, doi:10.1146/annurev.ea.23.050195.001343.

Pearce, J. A., P. E. Baker, P. K. Harvey, and I. W. Luff (1995), Geochemical evidence for subduction fluxes, mantle melting and fractional crystallization beneath the South Sandwich island arc, *J. Petrol.*, *36*, 1073–1109, doi:10.1093/petrology/36.4.1073.

Rapp, R. P., N. Shimizu, M. D. Norman, and G. S. Applegate (1999), Reaction between slab-derived melts and peridotite in the mantle wedge: experimental constraints at 3.8 GPa, *Chem. Geol.*, *160*, 335–356, doi:10.1016/S0009-2541(99)00106-0.

Rollinson, H. R. (1993), *Using Geochemical Data: Evaluation, Presentation, Interpretation*, Longman Singapore Publisher (Pte), Singapore.

Rudnick, R. L., and S. Gao (2003), Composition of the continental crust, in *Treatise on Geochemistry*, edited by H. D. H. Holland and K. K. Turekian, pp. 1–64, Elsevier-Pergamon, Oxford.

Santosh, M., D. Zhao, and T. Kusky (2010), Mantle dynamics of the Paleoproterozoic North China Craton: A perspective based on seismic tomography, *J. Geodynamics*, *49*, 39–53, doi:10.1016/j.jog.2009.09.043.

Sláma, J., et al. (2008), Plešovice zircon – A new natural reference material for U–Pb and Hf isotopic microanalysis, *Chem. Geol.*, *249*, 1–35, doi:10.1016/j.chemgeo.2007.11.005.

Stern, C. R., and R. Kilian (1996), Role of the subducted slab, mantle wedge and continental crust in the generation of adakites from the Andean Austral Volcanic Zone, *Contrib. Mineral. Petrol.*, *123*, 263–281, doi:10.1007/s004100050155.

Sun, S. S., and W. F. McDonough (1989), Chemical and isotopic systematic of oceanic basalt: implication for mantle composition and processes, in *Magmatism in the oceanic basins*, edited by A. D. Saunders and M. J. Norry, pp. 313–345, Geological Society Special Publication, Oxford.

Sun, W., X. Ding, Y. H. Hu, and X. H. Li (2007), The golden transformation of the Cretaceous plate subduction in the west Pacific, *Earth Planet. Sci. Lett.*, *262*, 533–542, doi:10.1016/j.epsl.2007.08.021.

Tang, Y. J., H. F. Zhang, and J. F. Ying (2006), Asthenosphere-lithospheric mantle interaction in an extensional regime: Implication from the geochemistry of Cenozoic basalts from Taihang Mountains, North China Craton, *Chem. Geol.*, *233*, 309–327, doi:10.1016/j.chemgeo.2006.03.013.

Tang, Y. J., H. F. Zhang, M. Santosh, and J. F. Ying (2013), Differential destruction of the North China Craton: A tectonic perspective, *J. Asian Earth Sci.*, doi:10.1016/j.jseaes.2012.11.047.

Tang, Y. J., H. F. Zhang, E. Deloule, B. X. Su, J. F. Ying, Y. Xiao, and Y. Hu (2012), Slab-derived lithium isotopic signatures in mantle xenoliths from northeastern North China Craton, *Lithos*, *149*, 79–90, doi:10.1016/j.lithos.2011.12.001.

Wang, Q., D. A. Wyman, J. F. Xu, Z. H. Zhao, P. Jian, X. L. Xiong, Z. W. Bao, C. F. Li, and Z. H. Bai (2006), Petrogenesis of Cretaceous adakitic and shoshonitic igneous rocks in the Luzong area, Anhui Province (eastern China): Implications for geodynamics and Cu-Au mineralization, *Lithos*, *89*, 424–446, doi:10.1016/j.lithos.2005.12.010.

Wang, Y. L., Q. Zhang, and Y. Wang (2001), Geochemical characteristics of volcanic rocks from Ningwu area, and its significance, *Acta Petro. Sin.*, *17*, 565–575, in Chinese with English abstract.

Wu, F. Y., J. Q. Lin, S. A. Wilde, X. O. Zhang, and J. H. Yang (2005), Nature and significance of the Early Cretaceous giant igneous event in eastern China, *Earth Planet. Sci. Lett.*, *233*, 103–119, doi:10.1016/j.epsl.2005.02.019.

Wu, Y. B., and Y. F. Zheng (2013), Tectonic evolution of a composite collision orogen: An overview on the Qinling–Tongbai–Hong'an–Dabie–Sulu orogenic belt in central China, *Gondwana Res.*, doi:10.1016/j.gr.2012.09.007.

Xu, H., C. Ma, and K. Ye (2007), Early cretaceous granitoids and their implications for the collapse of the Dabie orogen, eastern China: SHRIMP zircon U–Pb dating and geochemistry, *Chem. Geol.*, *240*, 238–259, doi:10.1016/j.chemgeo.2007.02.018.

Xu, Y. G. (2001), Thermo-tectonic destruction of the Archean lithospheric keel beneath the Sino-Korean Craton in China: Evidence, timing and mechanism, *Phys. Chem. Earth (A)*, *26*, 747–757, doi:10.1016/S1464-1895(01)00124-7.

Xu, Y. G., H. H. Zhang, H. N. Qiu, W. C. Ge, and F. Y. Wu (2012), Oceanic crust components in continental basalts from Shuangliao, Northeast China: Derived from the mantle transition zone?, *Chem. Geol.*, *328*, 168–184, doi:10.1016/j.chemgeo.2012.01.027.

Yan, J., J. F. Chen, and X. S. Xu (2008), Geochemistry of Cretaceous mafic rocks from the Lower Yangtze region, eastern China: Characteristics and evolution of the lithospheric mantle, *J. Asian Earth Sci.*, *33*, 177–193, doi:10.1016/j.jseaes.2007.11.002.

Yan, J., H. Q. Liu, C. Z. Song, X. S. Xu, Y. J. An, J. Liu, and L. Q. Dai (2009), Zircon U-Pb geochronology of the volcanic rocks from Fanchang-Ningwu volcanic basins in the Lower Yangtze region and its geological implications, *Chin. Sci. Bullet.*, *54*, 2895–2904, doi:10.1007/s11434-009-0110-x.

Yang, J. H., S. L. Chung, S. A. Wilde, F. Y. Wu, M. F. Chu, C. H. Lo, and H. R. Fan (2005), Petrogenesis of post-orogenic syenites in the Sulu Orogenic Belt, East China: geochronological, geochemical and Nd-Sr isotopic evidence, *Chem. Geol.*, *214*, 99–125, doi:10.1016/j.chemgeo.2004.08.053.

Yang, W. (2002), Geophysical profiling across the Sulu ultra-high-pressure metamorphic belt, eastern China, *Tectonophysics*, *354*, 277–288, doi:10.1016/S0040-1951(02)00386-4.

Zhang, H. F. (2005), Transformation of lithospheric mantle through peridotite-melt reaction: A case of Sino-Korean craton, *Earth Planet. Sci. Lett.*, *237*, 768–780, doi:10.1016/j.epsl.2005.06.041.

Zhang, H. F. (2009), Peridotite-melt interaction: A key point for the destruction of cratonic lithospheric mantle, *Chin. Sci. Bullet.*, *54*, 3417–3437, doi:10.1007/s11434-009-0307-z.

Zhang, H. F., L. Chen, M. Santosh, and M. A. Menzies (2013), Construction and destruction of cratons: Preface, *Gondwana Res.*, *23*, 1–3, doi:10.1016/j.gr.2012.06.006.

Zhang, H. F., S. Goldstein, X. H. Zhou, M. Sun, J. P. Zheng, and Y. Cai (2008), Evolution of subcontinental lithospheric mantle beneath eastern China: Re-Os isotopic evidence from mantle xenoliths in Paleozoic kimberlites and Mesozoic basalts, *Contrib. Mineral. Petrol.*, *155*, 271–293, doi:10.1007/s00410-007-0241-5.

Zhang, H. F., J. F. Ying, Y. J. Tang, X. H. Li, C. Feng, and M. Santosh (2011), Phanerozoic reactivation of the Archean North China Craton through episodic magmatism: Evidence from zircon U-Pb geochronology and Hf isotopes from the Liaodong Peninsula, *Gondwana Res.*, *19*, 446–459, doi:10.1016/j.gr.2010.09.002.

Zhang, J. J., Y. F. Zheng, and Z. F. Zhao (2009), Geochemical evidence for interaction between oceanic crust and lithospheric mantle in the origin of Cenozoic continental basalts in east-central China, *Lithos*, *110*, 305–326, doi:10.1016/j.lithos.2009.01.006.

Zhang, Q., P. Jian, D. Y. Liu, Y. L. Wang, Q. Qian, Y. Wang, and H. M. Xue (2003a), SHRIMP dating of volcanic rocks from Ningwu area and its geological implications, *Sci. in China (D)*, *46*, 830–837, doi:10.1360/03yd0310.

Zhang, Y., S. Dong, and W. Shi (2003b), Cretaceous deformation history of the middle Tan-Lu fault zone in Shandong Province, eastern China, *Tectonophysics*, *363*, 243–258, doi:10.1016/S0040-1951(03)00039-8.

Zhao, D., S. Maruyama, and S. Omori (2007), Mantle dynamics of Western Pacific and East Asia: Insight from seismic tomography and mineral physics, *Gondwana Res.*, *11*, 120–131, doi:10.1016/j.gr.2006.06.006.

Zheng, J. P., W. L. Griffin, S. Y. O'Reilly, C. M. Yu, H. F. Zhang, N. Pearson, and M. Zhang (2007), Mechanism and timing of lithospheric modification and replacement beneath the eastern North China Craton: Peridotitic xenoliths from the 100 Ma Fuxin basalts and a regional synthesis, *Geochim. Cosmochim. Acta*, *71*, 5203–5225, doi:10.1016/j.gca.2007.07.028.

Zheng, J. P., W. L. Griffin, S. Y. O'Reilly, J. S. Yang, T. F. Li, M. Zhang, R. Y. Zhang, and J. G. Liou (2006), Mineral chemistry of peridotites from Paleozoic, Mesozoic and Cenozoic lithosphere: Constraints on mantle evolution beneath eastern China, *J. Petrol.*, *47*, 2233–2256, doi:10.1093/petrology/egl042.

Zhou, T. F., Y. Fan, F. Yuan, L. J. Zhang, B. Qian, L. Ma, X. F. Yang, and D. R. Cook (2011), Geochronology and significance of volcanic rocks in the Ning-Wu basin of China, *Sci. China Earth Sci.*, *54*, 185–196, doi:10.1007/s11430-010-4150-5.

Zhou, X. M., and W. X. Li (2000), Origin of Late Mesozoic igneous rocks in Southeastern China: implications for lithosphere subduction and underplating of mafic magmas, *Tectonophysics*, *326*, 269–287, doi:10.1016/S0040-1951(00)00120-7.

Zhou, X. M., T. Sun, W. Z. Shen, L. S. Shu, and Y. L. Niu (2006), Petrogenesis of Mesozoic granitoids and volcanic rocks in South China: a response to tectonic evolution, *Episodes*, *29*, 26–33.

Zhu, R. X., Y. G. Xu, G. Zhu, H. F. Zhang, Q. K. Xia, and T. Y. Zheng (2012), Destruction of the North China Craton, *Sci. China Earth Sci.*, *55*, 1565–1587, doi:10.1007/s11430-012-4516-y.

Zindler, A., and S. R. Hart (1986), Chemical geodynamics, *Annu. Rev. Earth Planet. Sci.*, *14*, 493–571, doi:10.1146/annurev.ea.14.050186.002425.